JTTEE5 24:915–924
DOI: 10.1007/s11666-015-0251-1
1059-9630/$19.00 © ASM International

Titanium Dioxide Coating Prepared by Use of a Suspension-Solution Plasma-Spray Process

Lingzhong Du, Thomas W. Coyle, Ken Chien, Larry Pershin, Tiegang Li, and Mehdi Golozar

(Submitted August 1, 2013; in revised form April 29, 2015)

Titanium dioxide coatings were prepared from titanium isopropoxide solution containing nano TiO_2 particles by use of a plasma-spray process. The effects of stand-off distance on coating composition and microstructure were investigated and compared with those for pure solution precursor and a water-based suspension of TiO_2. The results showed that the anatase content of the coating increased with increasing stand-off distance and the rate of deposition decreased with increasing spray distance. Anatase nanoparticles in solution were incorporated into the coatings without phase transformation whereas most of the TiO_2 in the precursor solution was transformed into rutile. The microstructure of preserved anatase particles bound by rutile improved the efficiency of deposition of the coating. The amount of anatase phase can be adjusted by variation of the ratio of solution to added anatase TiO_2 nanoparticles.

Keywords plasma spray, solution, suspension, titanium dioxide

1. Introduction

Titanium dioxide (TiO_2) has a wide range of applications, for example in photovoltaic cells in solar energy conversion (Ref 1), as exhaust gas sensors in the automobile industry (Ref 2), as biomedical coatings in healthcare (Ref 3), and, especially, as one of the most important photocatalysts for elimination of organic compounds from polluted air and waste water (Ref 4). The photocatalytic activity of TiO_2 depends strongly on crystal phase, particle size, and specific surface area. Anatase and rutile are the two main crystalline phases of titanium dioxide. Anatase is a metastable phase that irreversibly transforms into rutile at high temperatures (Ref 5, 6). Although it is generally believed that anatase has better photocatalytic activity than rutile (Ref 4), some researchers have reported that rutile also has selective activity toward some compounds (Ref 7, 8). Ohno reported that TiO_2 powder containing both anatase and rutile particles had the highest activity in photocatalytic oxidation of naphthalene and that there was synergism between rutile and anatase (Ref 9–11). This suggests there may be an optimum ratio of rutile to anatase which yields the highest photocatalytic activity. Nanometer crystallite size is favored because of quantum size effects (Ref 12). A porous structure is also required to provide a large surface area for photocatalysis (Ref 13).

Not surprisingly, many techniques have been investigated for production of TiO_2 films and coatings, including use of sol–gel methods (Ref 14), chemical vapor deposition (Ref 15), chemical spray pyrolysis (Ref 16), plasma-spray deposition (Ref 17), and cold spraying (Ref 18). Among these, plasma-spray deposition has the advantages of a high rate of deposition, flexibility which enables coating of substrates of different shapes, and promising economic prospects for industrial scale-up (Ref 5).

Plasma power has important effects on microstructure, phase composition, and efficiency of deposition during the plasma-spray deposition of TiO_2 coatings. Low plasma power tends to produce a coating with high anatase content and porosity. However, the efficiency of deposition and the cohesive strength of the coating are generally low under these conditions, which inevitably increases the cost and limits the life of the coating. Increasing the plasma power improves the efficiency of deposition and cohesive strength, but results in a decrease in the anatase content of the coating, because of transformation of anatase into rutile during deposition (Ref 5, 19).

Rutile is the dominant phase in traditional plasma-sprayed coatings because of the high temperature of the particles in the plasma plume. Use of liquid feedstock is a promising modification of the conventional plasma-spray technique which enables deposition of nanostructured coatings (Ref 6). Two types of liquid feedstock have been used as precursors, suspensions of fine powders and solutions (Ref 20). The latter have the advantages of elimination of a separate powder preparation step and better

Lingzhong Du, State Key Laboratory of Multiphase Complex Systems, Institute of Process Engineering, Chinese Academy of Sciences, Beijing 100190, People's Republic of China and Centre for Advanced Coating Technologies, University of Toronto, Toronto, ON M5S 3G8, Canada; and **Thomas W. Coyle, Ken Chien, Larry Pershin, Tiegang Li,** and **Mehdi Golozar**, Centre for Advanced Coating Technologies, University of Toronto, Toronto, ON M5S 3G8, Canada. Contact e-mails: dulingzhong@hotmail.com and tom.coyle@utoronto.ca.

control of complex chemistry. In the solution precursor plasma-spray process, the solution precursor is injected into the plasma jet as a stream or after atomization. The liquid breaks up into fine droplets in the high-velocity plasma gas stream where the solvent evaporates, fine particles are formed from the solution precursor, and subsequently the particles may agglomerate, sinter, and perhaps melt before becoming deposited on the substrate to form a coating. Many studies of the deposition of TiO_2 coatings by use of the solution precursor (Ref 6, 21–23) or suspension thermal spray (Ref 24–33) methods have been reported.

In this research, TiO_2 anatase nanoparticles were dispersed in a titanium isopropoxide precursor solution to combine the merits of the precursor solution and suspension plasma spray methods an to obtain a titania coating with high deposition efficiency while retaining a high proportion of the anatase phase. The effects on coating phase composition and microstructure of stand-off distance and the relative amounts of solution and suspension injected into the plasma were investigated.

2. Experimental

2.1 Preparation of Precursor Solution

The solution was prepared by diluting 60.0 mL HCl (37%, Alfa Aesar, Canada) with 112.5 mL distilled deionized water and then adding 150 mL titanium isopropoxide ($Ti(OCH(CH_3)_2)_4$ (97%; Sigma–Aldrich, Canada) with vigorous stirring. The pH was kept below 2.0 to prevent hydrolysis of the titanium isopropoxide. The concentration of titanium isopropoxide in the resulting transparent precursor solution was 1.58 mol/L.

2.2 Suspension Preparation

The TiO_2 powder (MKnano, Mississauga, Canada) used to prepare the suspensions had an anatase content higher than 98% and an average particle size of 50 nm. Two suspensions were prepared for plasma spraying. One consisted of 60 g TiO_2 powder in 320 mL distilled deionized water. The other was 60 g TiO_2 powder in the precursor solution described above. PEI commercial dispersant (0.5 wt.%) was added to improve the stability of the suspensions. To prevent sedimentation the suspensions obtained were stirred continuously by use of a magnetic stirrer during the entire spraying process.

2.3 Coating Deposition

Coatings were prepared by use of a plasma spray system developed in the Centre for Advanced Coating Technologies, University of Toronto. Argon and carbon dioxide were used as the primary plasma gases, and CH_4 as the secondary plasma gas. The system has the advantages of high power and low cost, which are well suited for liquid feed stock plasma-spray processes. Coatings were deposited on stainless steel disk substrates 25 mm in diameter and 3 mm thick. The surface was grit blasted with Al_2O_3 grit (30 mesh) before deposition.

The liquid feedstock was fed to the nozzle from a closed tank, using Ar gas to pressurize the system. The liquid was radially injected as a continuous stream into the plasma jet 5 mm from the end of the torch through a 150 μm diameter orifice which was 15 mm from the jet axis. Four samples were sprayed simultaneously with stand-off distances of 7, 9, 11, and 13 cm. All coatings were deposited by use of the process conditions listed in Table 1. Twenty-four scans were performed with a linear torch velocity of 200 mm/s. Coatings were deposited by use of three types of liquid feedstock: precursor solution, TiO_2 nanoparticles + water, and TiO_2 nanoparticles + precursor solution, hereafter abbreviated as SP, NW, and NSP, respectively. Substrates were preheated by exposure to the plasma torch before the liquid feedstock was applied. Substrate temperatures were measured by use of a thermocouple in contact with the back of the substrate. A schematic diagram of the liquid feedstock plasma-spray process is shown in Fig. 1.

2.4 Characterization

Coated substrates were mounted by use of epoxy resin, then sectioned by use of a diamond saw. The specimens

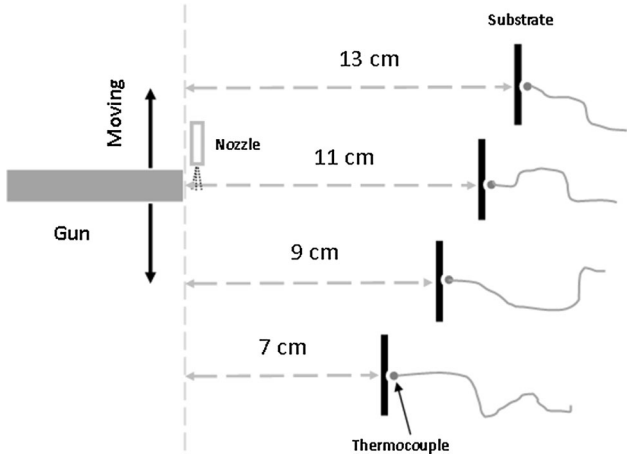

Fig. 1 Schematic diagram of the liquid feedstock plasma-spray process

Table 1 Conditions of the plasma-spray process

Plasma power, kW	Atomizing gas pressure, MPa	Suspension flow rate, mL/min	Ar flow, L/min	CO_2 flow, L/min	CH_4 flow, L/min
33	0.345	21	10	14	5

were ground to a 1200-grit finish and polished with 1 μm diamond paste. The thickness and microstructure of the coatings were characterized by scanning electron microscopy (JSM-840; Jeol, Tokyo, Japan).

The composition of the crystalline phase of the coatings was determined by x-ray diffraction with Cu Kα radiation (XRD; Philips, Eindhoven, The Netherlands). The XRD patterns were collected in the 2θ angle range from 20° to 60° with a scanning rate of 1.2°/min.

Micro-Raman analysis was performed by use of a Renishaw InVia Reflex spectrometer (Renishaw, Wotton-under-Edge, UK); the attached microscope was a Leica DMLM. Sample excitation was achieved by use of a solid laser emitting at 532 nm. To avoid sample heating or phase transformation, measurements were performed at a low excitation power (<4 mW on the surface of the sample). Samples were scanned from 100 to 1200 cm^{-1} wavenumber shift at a spectral resolution of 2 cm^{-1}.

3. Results

3.1 Crystalline Phases

Figure 2 shows the diffraction patterns of SP, NW and NSP coatings obtained at stand-off distances of 7, 9, 11, and 13 cm.

The volume percentage of anatase can be simply determined by use of the relationship given by Berger-Keller et al. (Ref 19)

$$C_A = \frac{8I_A}{8I_A + 13I_R} \quad \text{(Eq 1)}$$

where I_A and I_R are the XRD peak intensity of anatase (101) at 2θ = 25.4° and rutile (110) at 2θ = 27.4°, respectively.

The calculated volume percentages of anatase are plotted as a function of stand-off distance in Fig. 3. It can be seen that the percentage of anatase was strongly related to the stand-off distance and the type of the liquid feedstock. The anatase content increased with stand-off distance for all SP, NSP, and NW coatings. It seems that this increase was faster for NSP and NW than for SP. The anatase content of SP coatings was the lowest among the three types of coating; even the highest value at the stand-off distance of 13 cm was only 23%. The anatase content of NW coatings was the highest. The value at a stand-off distance of 7 cm was 48.5%, increasing to 90% at the stand-off distance of 13 cm.

3.2 Microstructure of the Coatings

SEM images of polished cross-sections of the SP, NW, NSP coatings at the four stand-off distances are shown in Fig. 4, 5, and 6. Coating morphology is highly dependent on the type of liquid feedstock and the stand-off distance.

The SP coatings (Fig. 4) consisted of high density regions of size 10–20 μm interspersed among large pores. The size and area fraction of the high-density regions decreased with increasing stand-off distance. The dense

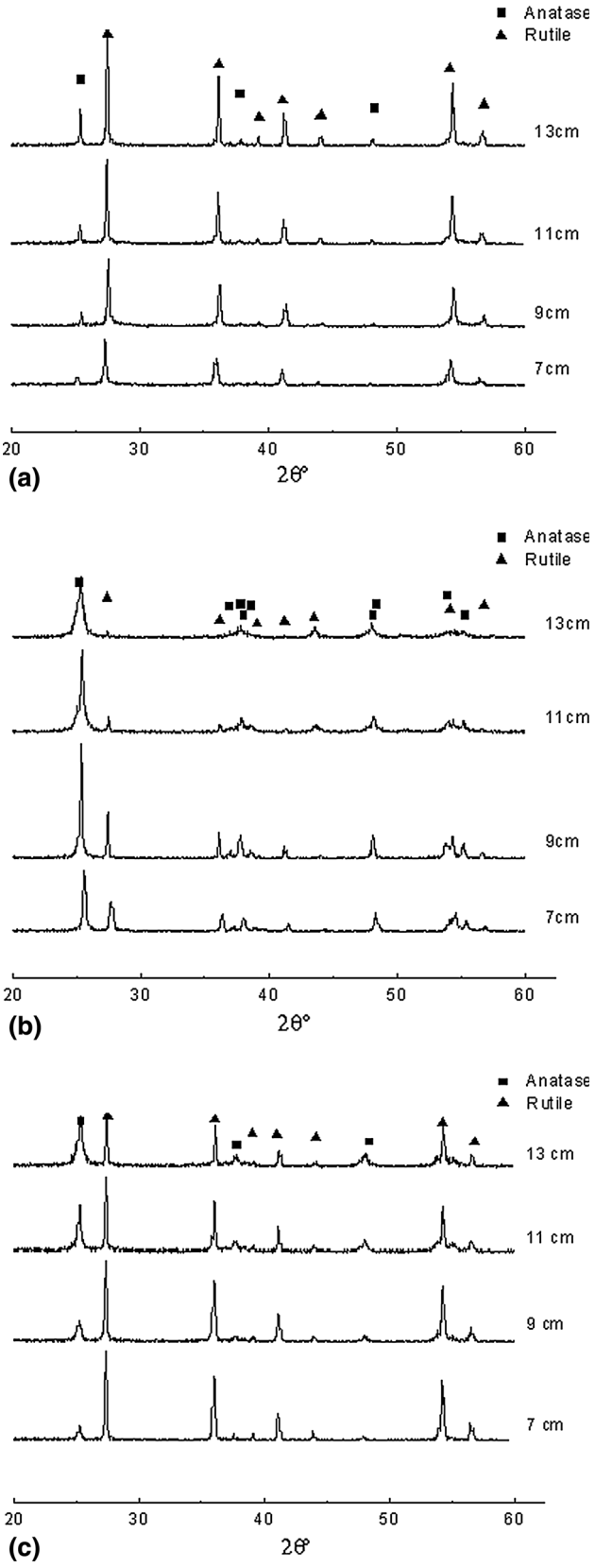

Fig. 2 XRD patterns of three types of coatings with different stand-off distance: (a) from pure solution precursor, (b) from water-based suspension, and (c) from solution precursor based suspension

regions were largely made up of equiaxed particles or grains, with only an occasional splat-shaped feature. As the stand-off distance was increased an increasing number of dense, spherical particles of diameter 2–4 μm were observed. There were no obvious cracks.

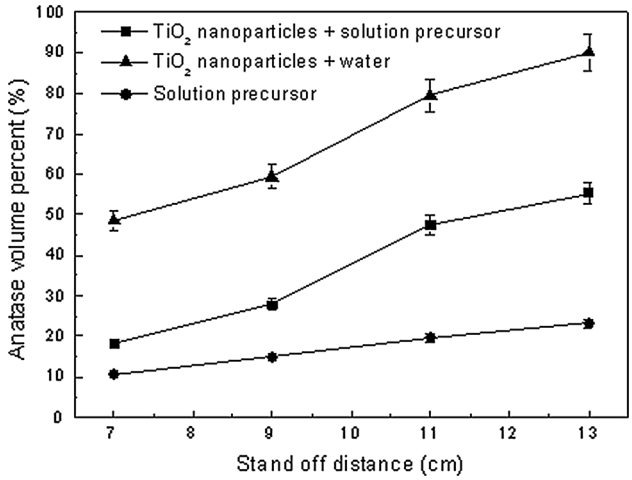

Fig. 3 Calculated anatase content for three types of coatings as a function of stand-off distance

Equiaxed dense regions 5–10 μm in size scattered in a dark gray matrix were observed in the NW coatings (Fig. 5). The dark gray region consisted of packed nanoparticles, whose size was the same as the starting powder. The dense fraction in the coatings decreased rapidly with increasing stand-off distance, and consisted only of isolated, spherical particles 2-4 μm in diameter for the two longest stand-off distances.

The NSP coatings (Fig. 6) were mainly composed of agglomerated nanoparticles with irregularly shaped dense regions scattered throughout. The fine pores were distributed homogeneously throughout the coatings, which would result in a large specific surface area suitable for use as a photocatalyst. The coating was denser close to the surface than adjacent to the substrate.

The density and thickness of the SP, NW, and NSP coatings decreased with increasing stand-off distance (Fig. 7). The spray distance had greater effect on the thickness of the NW coatings than on that of the SP and NSP coatings. The thickness of the NW coatings decreased by almost 80% when the spray distance was increased from 7 to 9 cm. The NSP coatings were the thickest of the

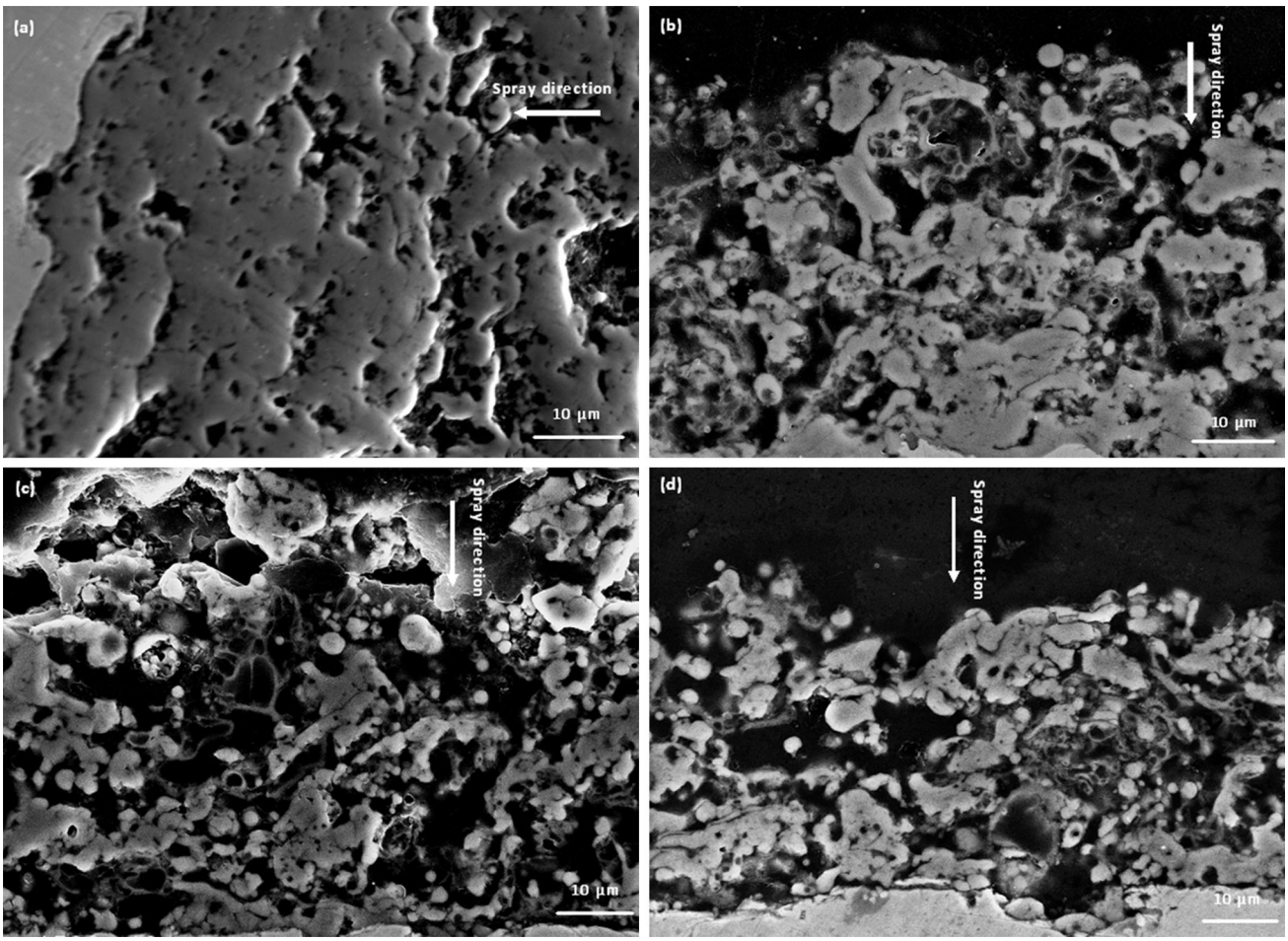

Fig. 4 Morphology of polished cross-sections of the coatings obtained from pure solution precursor with different stand-off distances: (a) 7 cm, (b) 9 cm, (c) 11 cm, and (d) 13 cm

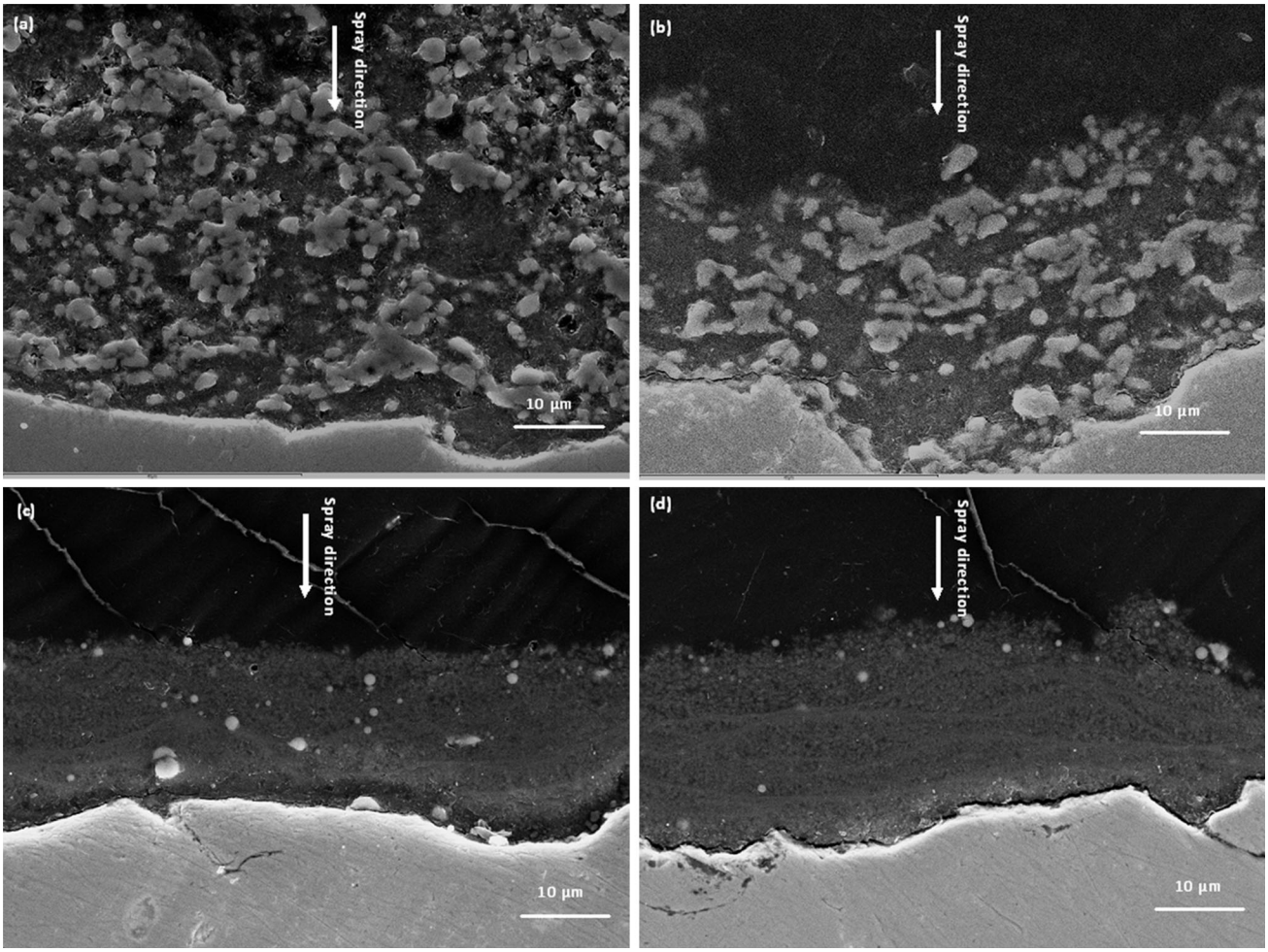

Fig. 5 Morphology of polished cross-sections of the coatings obtained from water-based suspensions with different stand-off distances: (a) 7 cm, (b) 9 cm, (c) 11 cm, and (d) 13 cm

three types of coating; thickness was greater than the sum of the NW and SP coatings under the same conditions.

3.3 Raman Spectroscopy

Micro-Raman measurements were performed to identify the phases in the coatings. A typical spectrum obtained from the bright dense regions in Fig. 4, 5, and 6 is shown in Fig. 8a. It contains Raman-active bands at 143 cm^{-1} (B_{1g}), 448 cm^{-1} (E_g), and 612 cm^{-1} (A_{1g}), which indicates the bright region is rutile (Ref 34). The spectrum obtained from the dark gray region (Fig. 8b) contains bands at 144 cm^{-1} (E_g), 197 cm^{-1} (E_g), 399 cm^{-1} (B_{1g}), 513 cm^{-1} (A_{1g}), and 639 cm^{-1} (E_g) (Fig. 8b), indicating this region is anatase (Ref 35).

4. Discussion

The microstructure and anatase content of suspension and solution spray titania coatings are highly dependent on thermal spray conditions, for example power (Ref 31), stand-off distance, liquid injection mode (internal or external) (Ref 29), solvent type (Ref 23), liquid feed rate, and the mass loading of particles in the suspension or the concentration of solution precursor (Ref 6, 21). This is why such great differences of porosity and anatase content have been reported in the literature. Porous or dense, high anatase content (up to 80%, Ref 28) or low anatase content (lower than 20%, Ref 29) coatings have been reported by different researchers. However, a coating with, simultaneously, a high anatase content, high deposition efficiency, and high cohesive strength has not been reported.

Two stages in the deposition process affect the microstructure and phase composition of a suspension or solution plasma-sprayed titania coating—exposure of the droplets and particles to the plasma jet in-flight and the heat treatment of the deposit during subsequent passes of the torch. When the liquid stream of the precursor solution or suspension is injected into the plasma jet, it is rapidly fragmented into droplets a few tens micrometers in diameter. The viscosity and surface tension of liquid affect the droplet size, and subsequent in-flight evolution of the droplets will differ for the SP, NW, and NSP liquids.

The SP precursor solution contained a high molar concentration of titanium isopropoxide, which, as the HCl

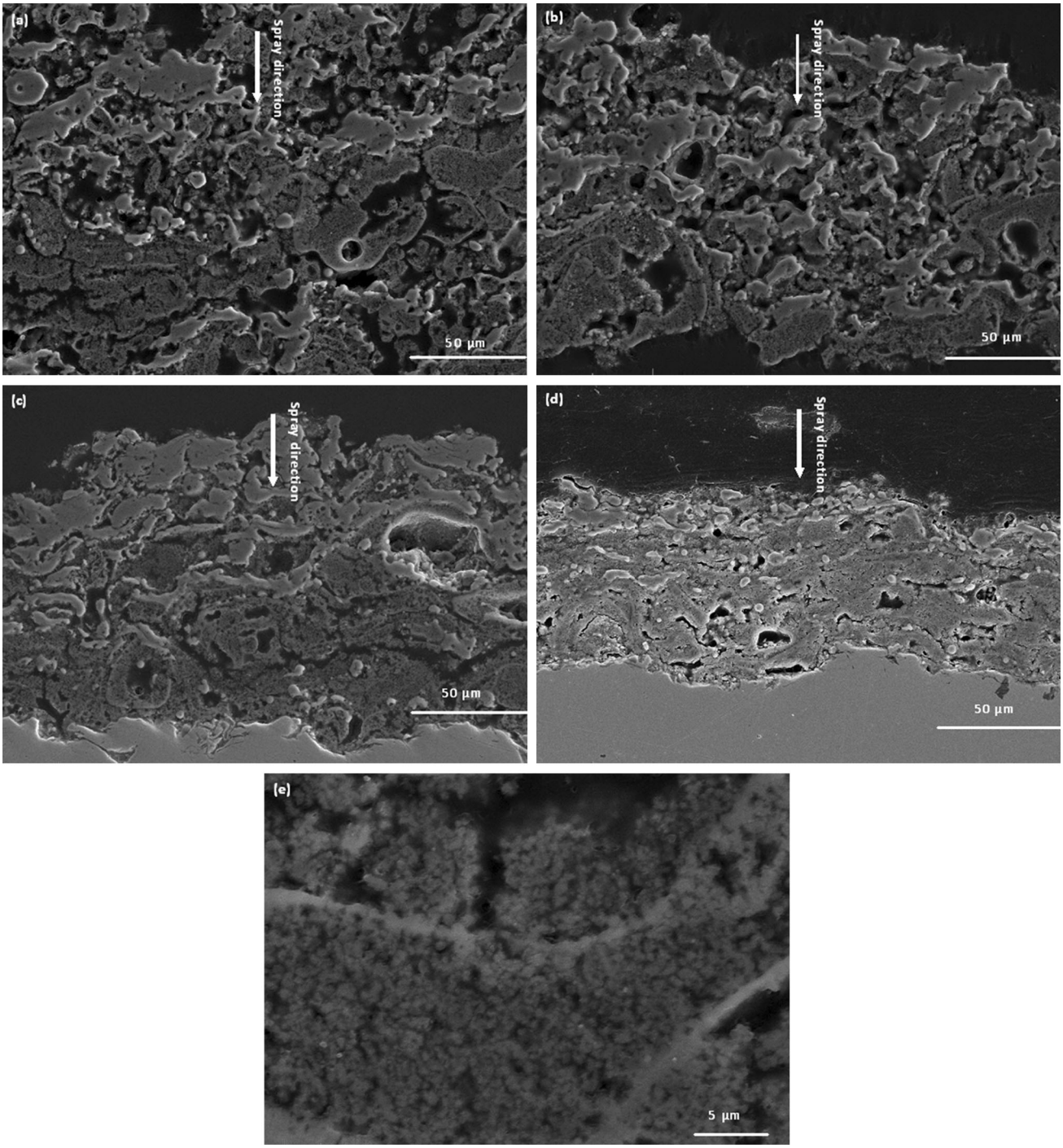

Fig. 6 Morphology of polished cross-sections of the coatings obtained from solution precursor-based suspensions with different stand-off distances: (a) 7 cm, (b) 9 cm, (c) 11 cm, and (d) 13 cm; (e) 7 cm, high magnification of (a)

stabilizer was volatilized, would be hydrolyzed in the plasma jet in accordance with the equation:

$$\mathrm{Ti(OCH(CH_3)_2)_4 + 2H_2O \rightarrow TiO_2 + 4\,(CH_3)_2CHOH.} \quad \text{(Eq 2)}$$

The ethyl alcohol produced would vaporize more quickly than water, and may undergo an exothermic combustion reaction with oxygen from decomposed H_2O or become entrained in the plasma from the surrounding air, increasing the enthalpy available for further evaporation, decomposition, pyrolysis, and melting of product phases. The liquid–solid interfacial energy of the anatase is lower than that of rutile, so anatase was likely to nucleate first (Ref 26), subsequently transforming to rutile as a result of further in-flight heating and possibly after deposition.

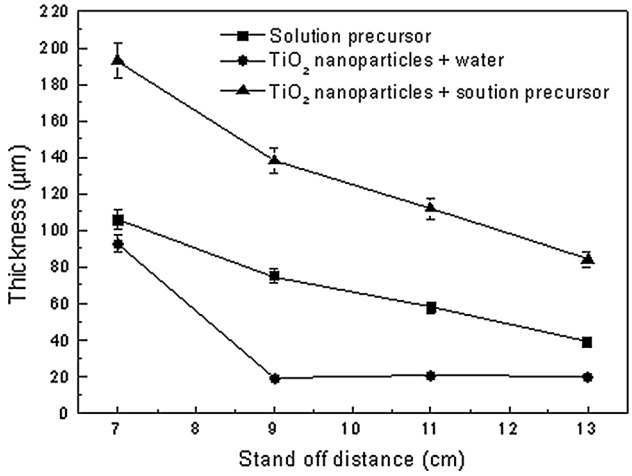

Fig. 7 Thickness of the three types of coating as a function of stand-off distance

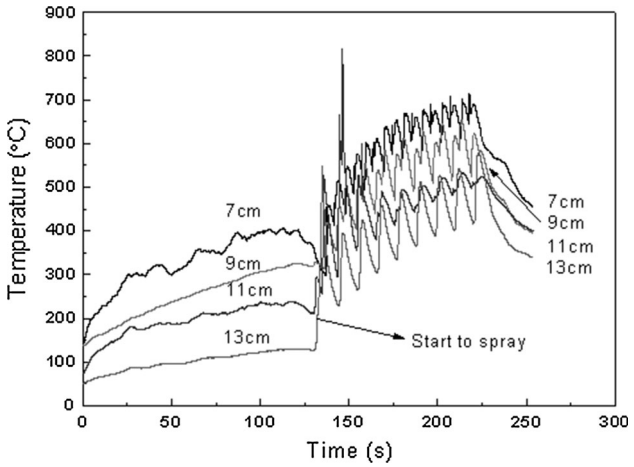

Fig. 9 Temperature of substrate as a function of plasma spray time for different stand-off distances

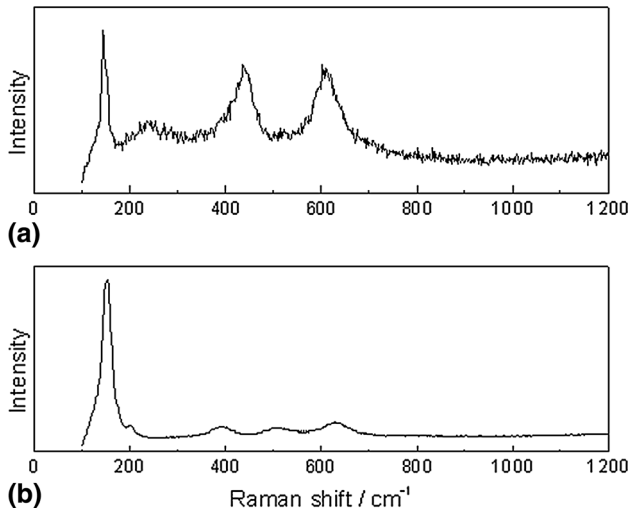

Fig. 8 Raman spectroscopy of (a) bright fraction and (b) dark gray fraction in the coating

Evaporation of water from the NW suspension (evaporation enthalpy 2.4×10^6 J/kg) would consume more energy than required for ethyl alcohol (0.6×10^6 J/kg) (Ref 31, 36), so the plasma plume would be expected to be cooler than for the SP solution. It seems that the plasma jet did not contain sufficient energy to induce transformation of the anatase particles in-flight, because a very high ratio of anatase phase (90% at a stand-off distance of 13 cm) was preserved in the coating. This phenomenon was also reported by Toma et al. during plasma spray and HVOF spray deposition of water-based suspensions of TiO_2 (Ref 28, 30, 31, 37) and by Kozerski and co-workers during the plasma-spray deposition of water-based hydroxyapatite suspension (Ref 26, 38). After deposition, the heat treatment by the plasma torch began to have an effect on phase transformation. Because the stand-off distance used in suspension or solution-plasma spraying (5–9 cm) is much shorter than the conventional plasma spray (9–11 cm), the heat flux from the torch to the deposited coating and substrate was extremely large (one order of magnitude higher than for conventional spraying (Ref 39). So the temperature of the substrate increased very quickly with the plasma jet repeatedly scanning over the substrate, as observed in Fig. 9. The shorter the standoff distance, the faster the temperature increase. When the temperature exceeded 600 °C, remaining anatase was readily converted into rutile because of the high surface energy of nanocrystalline anatase (Ref 11). The coating at a shorter stand-off distance suffered more from the effect of heat; as a result its anatase content is less.

The SP coating was mainly composed of well-melted rutile particles whereas the NW coating predominantly consisted of the unmelted anatase nanoparticle. If they could be combined, the rutile-to-anatase ratio could be controlled. This was evident from the NSP experiments, which furnished coatings consisting of unmelted anatase from added nanoparticles and melted rutile from the solution precursor, as is apparent from Fig. 6. During the plasma spraying, the solution precursor in the droplets of NSP went through the solvent evaporation, solute precipitation, pyrolysis, and phase transformation stages, as observed for the SP. The added anatase nanoparticles may need more energy to be transformed to rutile, because of the low activity compared with in situ anatase particles from the precursor solution, so most of these only agglomerated together and were subsequently incorporated into the coating. Stacks of individual lamellae built up a rutile–anatase composite coating, the so-called ''bimodal microstructure'' of many researchers (Ref 3, 40). The unmelted initial nanostructured anatase was tightly bound by the well-melted rutile from the solution precursor (Fig. 6e); in this way the cohesive strength of the coating could also be improved. Stuck by the solution precursor, more initial anatase particles could be trapped in the coating compared with NW spraying; the deposition efficiency of NSP was, thus, higher than the sum of SP and NW.

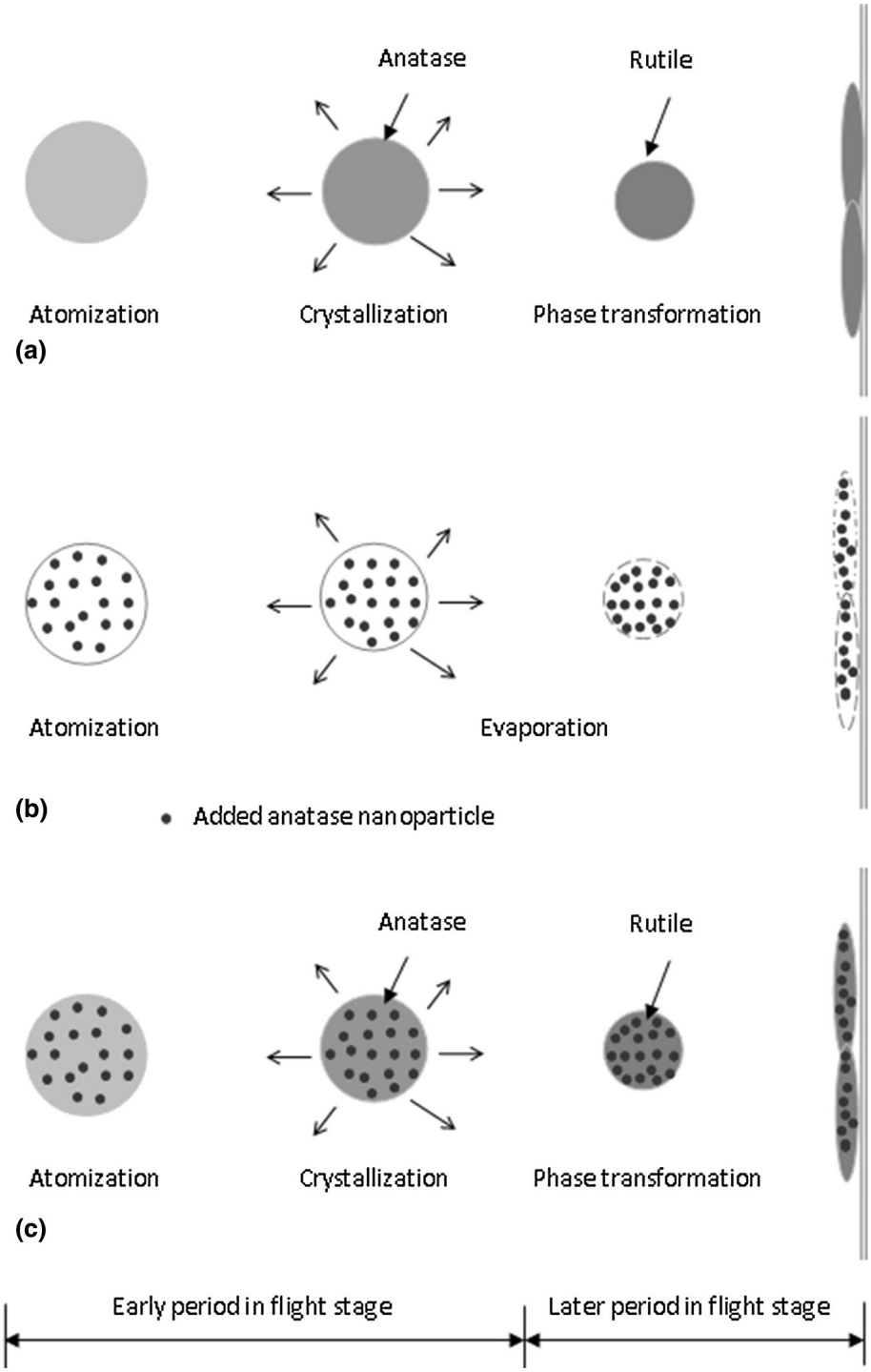

Fig. 10 Schematic diagrams of the evolution of: (a) the solution precursor, (b) the water-based suspension, and (c) the solution precursor-based suspension

On the basis of this analysis, deposition models for SP, NW, and NSP are shown schematically in Fig. 10. In the early period of the flight stage, isopropoxide hydrolyzed and nucleated to form anatase phase for SP and NSP, whereas water evaporation was the main phenomenon for NW because of the high heat absorption capacity of water. In the late period of the flight stage, parts of the formed anatase were converted into rutile for SP and NSP whereas most of the anatase was unchanged for NW, because of the cooling effect of water. The remaining anatase was partly transformed to rutile in the plasma plume during subsequent scanning with the plasma jet.

The stand-off distance also had important effects on coating deposition and microstructure. As measured by Marchand and Mauer et al. (Ref 41-43), the drops of the suspension reached their maximum velocities and temperature approximately 40–50 mm downstream of the *X*-axis of the plasma torch. There was then a rapid decrease in their velocities and temperature. So the deposition rate and density of the coatings decreased with stand-off distance, which was also observed by Cotler et al. during suspension plasma spray of titania, alumina, and YSZ (Ref 44). Combustion of the ethyl alcohol produced Increased the energy of the plasma and consequently increased the plasma temperature and velocity (Ref 40). Thus the effect of stand-off distance on the rate of deposition for SP and NSP was less than that for NW. The stand-off distance also had a large effect on coating phase composition. A long stand-off distance reduced the effect of plume heat on the deposited coating, thus reducing the transformation from anatase to rutile. As the temperature of the substrate increased with the time during spraying, the particles readily deformed on the hot substrate, the coatings became dense with increasing thickness. Improving the cooling conditions or intermittent spraying should suppress phase transformation and increase the anatase content in the coating.

Melting of the solution precursor reduced the porosity and improved the cohesive strength of the coating. The preserved initial nanostructured anatase ensured photocatalytic activity. So, it is possible to adjust the microstructure and properties of the coating by adjusting the ratio of solution precursor to added nanoparticles. This seems a promising way of preparing nanostructured coatings with high cohesive strength, high deposition efficiency, and controlled anatase content by the plasma spraying solution precursor-based suspension of anatase nanoparticles.

5. Conclusions

(1) The coating obtained from the water-based suspension had a high anatase content, because of the quenching effect of water on the plasma jet; use of the titanium isopropoxide precursor solution resulted in a high rate of deposition because of combustion of ethyl alcohol from pyrolysis of the precursor.

(2) The stand-off distance had an important effect on the rate of deposition and on phase structure of the coating. The rate of deposition decreased with increasing stand-off distance and the anatase content of the coatings increased with increasing spray distance.

(3) Addition of nanoparticles to the solution precursor increased the efficiency of deposition of the as-sprayed coating. The thickness of the coating was more than the sum of the coatings prepared from the pure solution and from the aqueous suspension.

(4) Most of the initial anatase particles were retained in the coating, whereas the TiO_2 in the precursor solution was transformed into rutile. The structure of the unmelted anatase surrounding the melted rutile improved the cohesive strength of the coating.

Acknowledgments

Financial support by the National Natural Science Foundation of China (grant no. 50901071) and the Innovation Fund Project of the Chinese Academy of Sciences (grant no. CXJJ-09-M56) is appreciated. The authors also thank George Kretschmann and Yanan Liu of the Department of Geology, University of Toronto, for their help during XRD and SEM characterization.

References

1. B. O'Regan, M. Gratzel, and A. Low-Cost, High-Efficiency Solar Cell Based on Dye-Sensitized Colloidal TiO_2 Films, *Nature*, 1991, **353**(6346), p 737-740
2. O.K. Varghese, D. Gong, M. Paulose, K.G. Ong, and C.A. Grimes, Hydrogen Sensing Using Titania Nanotubes, *Sens. Actuators B*, 2003, **93**(1-3), p 338-344
3. R. Lima and B. Marple, Thermal Spray Coatings Engineered from Nanostructured Ceramic Agglomerated Powders for Structural, Thermal Barrier and Biomedical Applications: A Review, *J. Therm. Spray Technol.*, 2007, **16**(1), p 40-63
4. A.L. Linsebigler, G. Lu, and J.T. Yates, Photocatalysis on TiO_2 Surfaces: Principles, Mechanisms, and Selected Results, *Chem. Rev.*, 1995, **95**(3), p 735-758
5. Z.B.Z.E. García, T.W. Coyle, S.E. Hao, and S.L. Mu, Liquid Precursors Plasma Spraying of TiO_2 and Ce-Doped $Ba(Zr_{0.2}Ti_{0.8})O_3$ Coatings, *Thermal Spray 2007: Global Coating Solutions*, B.R. Marple, M.M. Hyland, Y.-C. Lau, C.-J. Li, R.S. Lima, and G. Montavon, Ed., ASM International, Beijing, 2007, p 650-654
6. D. Chen, E.H. Jordan, and M. Gell, Porous TiO_2 Coating Using the Solution Precursor Plasma-spray process, *Surf. Coat. Technol.*, 2008, **202**(24), p 6113-6119
7. F.L. Toma, G. Bertrand, S.O. Chwa, C. Meunier, D. Klein, and C. Coddet, Comparative Study on the Photocatalytic Decomposition of Nitrogen Oxides Using TiO_2 Coatings Prepared by Conventional Plasma Spraying and Suspension Plasma Spraying, *Surf. Coat. Technol.*, 2006, **200**(20-21), p 5855-5862
8. M.R. Hoffmann, S.T. Martin, W. Choi, and D.W. Bahnemann, Environmental Applications of Semiconductor Photocatalysis, *Chem. Rev.*, 1995, **95**(1), p 69-96
9. T. Ohno, K. Tokieda, S. Higashida, and M. Matsumura, Synergism Between Rutile and Anatase TiO_2 Particles in Photocatalytic Oxidation of Naphthalene, *Appl. Catal. A*, 2003, **244**(2), p 383-391
10. D.C. Hurum, A.G. Agrios, K.A. Gray, T. Rajh, and M.C. Thurnauer, Explaining the Enhanced Photocatalytic Activity of Degussa P25 Mixed-Phase TiO_2 Using EPR, *J. Phys. Chem. B*, 2003, **107**(19), p 4545-4549
11. J. Jang, H. Takana, Y. Ando, O.P. Solonenko, and H. Nishiyama, Preparation of Carbon-Doped TiO_2 Nanopowder Synthesized by Droplet Injection of Solution Precursor in a DC-RF Hybrid Plasma Flow System, *J. Therm. Spray Technol.*, 2013, **22**(6), p 974-982
12. T.M.R. Viseu, B. Almeida, M. Stchakovsky, B. Drevillon, M.I.C. Ferreira, and J.B. Sousa, Optical Characterisation of Anatase: A Comparative Study of the Bulk Crystal and the Polycrystalline Thin Film, *Thin Solid Films*, 2001, **401**(1-2), p 216-224

13. M. Law, L.E. Greene, J.C. Johnson, R. Saykally, and P. Yang, Nanowire Dye-Sensitized Solar Cells, *Nat. Mater.*, 2005, **4**(6), p 455-459
14. J.B. Christophe, F. Arendse, P. Comte, M. Jirousek, F. Lenzmann, V. Shklover, and M. Gratzel, Nanocrystalline Titanium Oxide Electrodes for Photovoltaic Applications, *J. Am. Ceram. Soc.*, 1997, **80**(12), p 3157-3171
15. M. Zhou and X. Ma, Efficient Photoelectrocatalytic Activity of TiO_2/Ti Anode Fabricated by Metalorganic Chemical Vapor Deposition (MOCVD), *Electrochem. Commun.*, 2009, **11**(4), p 921-924
16. C. Natarajan, N. Fukunaga, and G. Nogami, Titanium Dioxide Thin Film Deposited by Spray Pyrolysis of Aqueous Solution, *Thin Solid Films*, 1998, **322**(1-2), p 6-8
17. H. Chen, S.W. Lee, T.H. Kim, and B.Y. Hur, Photocatalytic Decomposition of Benzene with Plasma Sprayed TiO_2-Based Coatings on Foamed Aluminum, *J. Eur. Ceram. Soc.*, 2006, **26**(12), p 2231-2239
18. G.-J. Yang, C.-J. Lia, F. Hana, W.-Y. Lia, and A. Ohmorib, Low Temperature Deposition and Characterization of TiO_2 Photocatalytic Film Through Cold Spray, *Appl. Surf. Sci.*, 2008, **254**(13), p 3979-3982
19. N. Berger-Keller, G. Bertrand, C. Filiatre, C. Meunier, and C. Coddet, Microstructure of Plasma-Sprayed Titania Coatings Deposited from Spray-Dried Powder, *Surf. Coat. Technol.*, 2003, **168**(2-3), p 281-290
20. L. Pawlowski, Suspension and Solution Thermal Spray Coatings, *Surf. Coat. Technol.*, 2009, **203**(19), p 2807-2829
21. D. Chen, E.H. Jordan, M. Gell, and X. Ma, Dense TiO_2 Coating Using the Solution Precursor Plasma-spray process, *J. Am. Ceram. Soc.*, 2008, **91**(3), p 865-872
22. D. Chen, E.H. Jordan, M. Gell, and M. Wei, Apatite Formation on Alkaline-Treated Dense TiO_2 Coatings Deposited Using the Solution Precursor Plasma-spray process, *Acta Biomater.*, 2008, **4**(3), p 553-559
23. D. Chen, E. Jordan, and M. Gell, Solution Precursor Plasma Spray Coatings: Influence of Solvent Type, *Plasma Chem. Plasma Process.*, 2010, **30**(1), p 111-119
24. G. Bolelli, V. Cannillo, R. Gadow, A. Killinger, L. Lusvarghi, and J. Rauch, Properties of High Velocity Suspension Flame Sprayed (HVSFS) TiO_2 Coatings, *Surf. Coat. Technol.*, 2009, **203**(12), p 1722-1732
25. E. Bemporad, G. Bolelli, V. Cannillo, D. De Felicis, R. Gadow, A. Killinger, L. Lusvarghi, J. Rauch, and M. Sebastiani, Structural Characterisation of High Velocity Suspension Flame Sprayed (HVSFS) TiO_2 Coatings, *Surf. Coat. Technol.*, 2010, **204**(23), p 3902-3910
26. R. Jaworski, L. Pawlowski, C. Pierlot, F. Roudet, S. Kozerski, and F. Petit, Recent Developments in Suspension Plasma Sprayed Titanium Oxide and Hydroxyapatite Coatings, *J. Therm. Spray Technol.*, 2010, **19**(1), p 240-247
27. R. Jaworski, L. Pawlowski, F. Roudet, S. Kozerski, and A. Maguer, Influence of Suspension Plasma Spraying Process Parameters on TiO_2 Coatings Microstructure, *J. Therm. Spray Technol.*, 2008, **17**(1), p 73-81
28. F.L. Toma, L.M. Berger, C. Stahr, T. Naumann, and S. Langner, Microstructures and Functional Properties of Suspension-Sprayed Al_2O_3 and TiO_2 Coatings: An Overview, *J. Therm. Spray Technol.*, 2010, **19**(1), p 262-274
29. S. Kozerski, F.-L. Toma, L. Pawlowski, B. Leupolt, L. Latka, and L.-M. Berger, Suspension Plasma Sprayed TiO_2 Coatings Using Different Injectors and Their Photocatalytic Properties, *Surf. Coat. Technol.*, 2010, **205**(4), p 980-986
30. F.L. Toma, L.M. Berger, D. Jacquet, D. Wicky, I. Villaluenga, Y.R. de Miguel, and J.S. Lindeløv, Comparative Study on the Photocatalytic Behaviour of Titanium Oxide Thermal Sprayed Coatings from Powders and Suspensions, *Surf. Coat. Technol.*, 2009, **203**(15), p 2150-2156
31. F.L. Toma, L.M. Berger, T. Naumann, and S. Langner, Microstructures of Nanostructured Ceramic Coatings Obtained by Suspension Thermal Spraying, *Surf. Coat. Technol.*, 2008, **202**(18), p 4343-4348
32. H. Podlesak, L. Pawlowski, J. Laureyns, R. Jaworski, and T. Lampke, Advanced Microstructural Study of Suspension Plasma Sprayed Titanium Oxide Coatings, *Surf. Coat. Technol.*, 2008, **202**(15), p 3723-3731
33. R. Jaworski, L. Pawlowski, F. Roudet, S. Kozerski, and F. Petit, Characterization of Mechanical Properties of Suspension Plasma Sprayed TiO_2 Coatings Using Scratch Test, *Surf. Coat. Technol.*, 2008, **202**(12), p 2644-2653
34. T. Ohsaka, F. Izumi, and Y. Fujiki, Raman Spectrum of Anatase, TiO_2, *J. Raman Spectrosc.*, 1978, **7**(6), p 321-324
35. S.P.S. Porto, P.A. Fleury, and T.C. Damen, Raman Spectra of TiO_2, MgF_2, ZnF_2, FeF_2, and MnF_2, *Phys. Rev.*, 1967, **154**(2), p 522-526
36. F.L. Toma, G. Bertrand, D. Klein, C. Coddet, and C. Meunier, Nanostructured Photocatalytic Titania Coatings Formed by Suspension Plasma Spraying, *J. Therm. Spray Technol.*, 2006, **15**(4), p 587-592
37. F.L. Toma, G. Bertrand, S. Begin, C. Meunier, O. Barres, D. Klein, and C. Coddet, Microstructure and Environmental Functionalities of TiO_2-Supported Photocatalysts Obtained by Suspension Plasma Spraying, *Appl. Catal. B*, 2006, **68**(1-2), p 74-84
38. S. Kozerski, L. Pawlowski, R. Jaworski, F. Roudet, and F. Petit, Two Zones Microstructure of Suspension Plasma Sprayed Hydroxyapatite Coatings, *Surf. Coat. Technol.*, 2010, **204**(9-10), p 1380-1387
39. P. Fauchais and G. Montavon, Latest Developments in Suspension and Liquid Precursor Thermal Spraying, *J. Therm. Spray Technol.*, 2010, **19**(1), p 226-239
40. P. Bansal, N.P. Padture, and A. Vasiliev, Improved Interfacial Mechanical Properties of Al_2O_3-13wt%TiO_2 Plasma-Sprayed Coatings Derived from Nanocrystalline Powders, *Acta Mater.*, 2003, **51**(10), p 2959-2970
41. O. Marchand, L. Girardot, M.P. Planche, P. Bertrand, Y. Bailly, and G. Bertrand, An Insight into Suspension Plasma Spray: Injection of the Suspension and Its Interaction with the Plasma Flow, *J. Therm. Spray Technol.*, 2011, **20**(6), p 1310-1320
42. A. Killinger, R. Gadow, G. Mauer, A. Guignard, R. Vaßen, and D. Stöver, Review of New Developments in Suspension and Solution Precursor Thermal Spray Processes, *J. Therm. Spray Technol.*, 2011, **20**(4), p 677-695
43. G. Mauer, A. Guignard, R. Vaßen, and D. Stöver, Process Diagnostics in Suspension Plasma Spraying, *Surf. Coat. Technol.*, 2010, **205**, p 961-966
44. E.M. Cotler, D. Chen, and R.J. Molz, Pressure-Based Liquid Feed System for Suspension Plasma Spray Coatings, *J. Therm. Spray Technol.*, 2011, **20**(4), p 967-973